

# RF current condensation in magnetic islands and associated hysteresis phenomena

Cite as: Phys. Plasmas **26**, 092511 (2019); doi: 10.1063/1.5118424

Submitted: 6 July 2019 · Accepted: 31 August 2019 ·

Published Online: 26 September 2019



View Online



Export Citation



CrossMark

E. Rodríguez,<sup>1,2,a)</sup> A. H. Reiman,<sup>1,2,b)</sup> and N. J. Fisch<sup>1,2,c)</sup>

## AFFILIATIONS

<sup>1</sup>Department of Astrophysical Sciences, Princeton University, Princeton, New Jersey 08543, USA

<sup>2</sup>Princeton Plasma Physics Laboratory, Princeton, New Jersey 08540, USA

<sup>a)</sup>Email: [eduardor@princeton.edu](mailto:eduardor@princeton.edu)

<sup>b)</sup>Email: [areiman@pppl.gov](mailto:areiman@pppl.gov)

<sup>c)</sup>Email: [fisch@princeton.edu](mailto:fisch@princeton.edu)

## ABSTRACT

The nonlinear RF current condensation effect suggests that magnetic islands might be well controlled with broader deposition profiles than previously thought possible. To assess this possibility, a simplified energy deposition model in a symmetrized 1D slab geometry is constructed. By limiting the RF wave power that can be absorbed through damping, this model also describes the predicted hysteresis phenomena. Compared to the linear model, the nonlinear effects lead to larger temperature variations, narrower deposition widths, and more robust island stabilization. Although, in certain regimes, the island center can be disadvantageously shaded because of the nonlinear effects, in general, the RF condensation effect can take place, with current preferentially generated, advantageously, close to the island center.

Published under license by AIP Publishing. <https://doi.org/10.1063/1.5118424>

## I. INTRODUCTION

Magnetic confinement approaches to fusion rely on the ordered topology of nested magnetic surfaces to prevent the plasma from escaping. Devices such as tokamaks and stellarators are designed toward this; however, in reality, magnetic fields are not perfect and are subject to resonant fields. These change the magnetic topology and result in magnetic islands appearing at rational surfaces.

Magnetic islands are characterized by flat density and temperature profiles due to enhanced transport through them. This reduction of pressure gradients suppresses bootstrap current within the island, generally making the island grow.<sup>1–4</sup> As a result, the confinement ability of the system decreases, paired with the occurrence of the so-called neoclassical tearing modes (NTMs).<sup>5</sup>

NTMs were recognized as a source of major disruptions in experiments such as JET,<sup>6,7</sup> and thus, their stabilization is central. Among the proposed stabilization approaches, driving current<sup>8,9</sup> at the islands with RF waves has stimulated a long list of added efforts,<sup>10–29</sup> including many experimental demonstrations.<sup>30–36</sup> By driving current at the center of the island using electron cyclotron (ECCD)<sup>37,38</sup> or lower hybrid current drive (LHCD),<sup>39,40</sup> one may balance the lack of bootstrap current and prevent the island growth.<sup>15</sup> This technique is, however, limited to its application to islands of smaller size due to available power constraints. This makes driving current precisely at

their center difficult, as the deposition width is comparable to the island size.

It has been recently suggested<sup>41</sup> that some of these stringent requirements may be relaxed due to the so-called “RF current condensation effect.” This effect takes into consideration the nonlinear feedback of temperature variations<sup>42</sup> resulting from RF wave heating onto the deposition itself. It was found that condensation could improve mitigation as well as reduce radial sensitivity.

Formally, in Ref. 41, this nonlinear feedback was modeled using a simplified diffusion energy balance equation that included resonant power deposition for a prescribed profile. Yet, the lack of a dissipation mechanism (e.g., radiation) or the unlimited absorbable power from RF waves, gave, as they observed, a nonphysical temperature blow-up beyond a bifurcation point. Here, that model is extended to include the damping of the RF wave.

In what follows, this extended model is first introduced in detail. Next, the equation is analytically and numerically solved and a hysteresis effect related to the island heating is described. Having introduced this phenomenon, the effects of the nonlinearities on different RF deposition schemes are explored. In order to evaluate these effects fairly, comparisons are made to the analytical linear solution, which is taken as a representative of current approaches.

## II. FUNDAMENTAL THEORETICAL MODEL

The model describes both the temperature variations of a magnetic island and the RF wave deposition. The latter may be described as a wave that is being damped along a ray trajectory, so as to provide the plasma with energy. The temperature of the plasma, driven by the RF waves, is described as part of an energy balance model with thermal diffusion. To construct such a model, various approximations are introduced.

Take, as a starting point, the transport equation,<sup>43</sup> representing the second moment of the Boltzmann equation, to describe temperature,  $T$ , dynamics. Under the assumption of no significant flows, and considering fast equilibration between electrons and ions, a single equation may be written combining the two-fluid Braginskii equations,

$$\frac{3}{2}nk_B\partial_t T - \nabla \cdot (\kappa \nabla T) = P, \quad (1)$$

where  $n$  is the plasma density,  $\kappa$  is the generalized heat conductivity tensor, and  $P$  is a volumetric power deposition which will be later related to the RF power input.

It has been stated as an assumption for Eq. (1) that electrons and ions are effectively equilibrated. Thus, the equation should only apply to those time scales larger than the typical equilibration time  $\tau_{\text{eq}}$ ; this constitutes the first temporal constraint:  $t \gg \tau_{\text{eq}}$ , where  $t$  denotes the time scales that the model is suited to describe.

A second point is related to the use of temperature as a measure of plasma energy. The concept of temperature customarily applies only to thermalized systems, in which the populations in  $v$ -space are Maxwellian distributed. However, the continuous injection of RF waves distorts the distribution function locally so as to deposit energy resonantly onto a small fraction of faster electrons (e.g., for lower hybrid (LH) waves,  $v \approx 4.5v_{Te}$  and for electron cyclotron (EC),  $v \approx 3v_{Te}$ ).<sup>38,44</sup> Hence, the plasma is made up of not only a Maxwellian bulk with a well defined  $T$  but also a resonant minority population. If the bulk  $T$  is to represent the total internal energy of the plasma, then the energy drawn locally in  $v$ -space needs to be redistributed quickly. Here, a second time ordering is introduced: collisional thermalization ( $\tau_{\text{se}}$ ) and isotropization ( $\tau_{\perp}$ ) processes must be faster than the time scales of interest ( $t \gg \tau_{\text{se}}, \tau_{\perp}$ ). In that case, non-Maxwellian features that affect a minute fraction of the total population may be ignored to leading order. The kinetic details will still prove important for  $P$ .

As it stands, Eq. (1) remains a three dimensional problem, but it may be cast into an approximate reduced 1D problem assuming the following. Consider as it happens (see Table I),<sup>42,45</sup> transport over a given magnetic flux surface to be much faster than perpendicular to it, that is,  $f_{\kappa} \equiv \kappa_{\parallel}/\kappa_{\perp} \gg 1$ . In that case, magnetic surfaces will be approximately isothermal, simplifying the derivatives in the diffusive term [i.e., the second term in Eq. (1)]. For analytical simplicity, the geometrical factor associated with the particular shape of island flux surfaces will be ignored, using instead a single slab coordinate  $x$  (one may think of making a cut to an elongated, narrow island). This reduced form is

$$\frac{3}{2}nk_B\partial_t T - \partial_x(\kappa_{\perp}\partial_x T) = P. \quad (2)$$

As a result of this slab adaptation, areal weighting is made equal for all points, though in reality this should be larger for the edges. A more

**TABLE I.** Summary of the various scales relevant to obtain the form of Eqs. (8a) and (8b) in typical tokamak parameters of  $T = 10$  keV,  $a = 1$  m,  $R = 5$  m,  $W_i = 0.05$  m,  $n = 10^{14}$  cm<sup>-3</sup>,  $\chi_{e\perp} = 0.5$  m<sup>2</sup> s<sup>-1</sup>,  $Z = 1$ , and  $q = 2$ .

Time scale	s
$\tau_{\text{se}}$	$1 \times 10^{-3}$
$\tau_{\perp}$	$1 \times 10^{-3}$
$\tau_D$	$3 \times 10^{-3}$
$\tau_E$	$8 \times 10^{-3}$
$\tau_{\text{eq}}$	$4 \times 10^{-1}$
$\tau_i$	1
$\tau_{\eta}$	$2 \times 10^2$
Dimensionless Scales	
$f_{\kappa}$	$10^{13}$
$\epsilon$	$10^{-1}$

complete treatment considering the flux coordinate is left for future work, though it was shown in Ref. 41 that the slab geometry shared the qualitative physics with the more realistic geometry.

Nonetheless, the model retains an important feature of the magnetic island geometry: the closed nature of magnetic surfaces about the island center. Consequently, in the reduced 1D model, temperature solutions are required to be even about the center  $x = 0$ .

Proceed now to linearize Eq. (2). Assume that the temperature changes ( $\tilde{T}$ ) in the island due to directing RF heating ( $P$ ) to it are small, i.e.,  $\epsilon = \tilde{T}/T_0 \ll 1$ , where  $T_0$  is the equilibrium temperature. Seeking precision in this definition,  $T_0$  is defined to be the island temperature when the RF power is not aimed directly at the island but is rather part of the total power budget that heats the center of the tokamak (see Fig. 1). Because  $T_0$  is constant over the island (as is the density), any island inhomogeneity that develops will be at least  $O(\epsilon)$ , and with this ordering, we drop derivatives with respect to  $\kappa_{\perp}$  in Eq. (2),

$$\frac{3}{2}nk_B\partial_t \tilde{T} - \kappa_{\perp}\partial_x^2 \tilde{T} = P. \quad (3)$$

The consideration of stiff temperature profiles that could modify  $\kappa_{\perp}$  nonsmoothly is left for future work.

To drop the time dependence of Eq. (3), the time scales of concern should exceed those of energy diffusion ( $\kappa_{\perp}\partial_x^2 \tilde{T}$  term) and the driving times ( $P$  term). Consider the former; clearly for the dominance of the diffusion term,  $t \gg \tau_D = W_i^2/\chi_{\perp}$ . Here,  $W_i$  represents the island width and  $\chi_{\perp} \approx \kappa_{\perp}/nk_B$  is the heat diffusion coefficient.

For the latter,  $nk_B\partial_t \tilde{T} \sim P$  suggests that the time derivative may be dropped, provided that the power density of the wave has had enough time to deposit all the needed thermal energy, i.e.,  $t \gg \tau_E = nk_B\Delta T/P$ , where  $\Delta T \sim \epsilon T_0$  is the characteristic variation of the island temperature. Then, with  $t$  in this regime, and being consistent with all of previous requirements,

$$-\kappa_{\perp}\partial_x^2 \tilde{T} = P. \quad (4)$$

Prior to detailing the form of  $P$ , the problem should be closed by both defining the spatial domain and setting appropriate boundary conditions. Naturally, one defines the last closed surface of the island

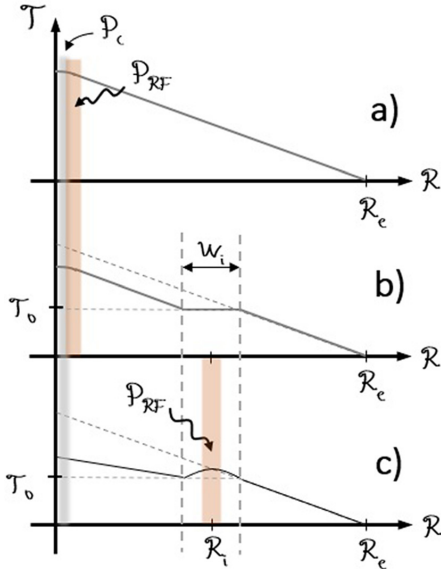


**FIG. 1.** Schematic sequence of temperature profiles of the full plasma for (a) no island present, (b) an island present at  $R = R_i$ , and (c) RF energy deposition displaced to within the island. The reddish band heating represents the region of RF deposition, while the gray one corresponds to other heating sources.

including the X-points as boundaries of the domain of  $x$ , i.e.,  $|x| \leq W_i/2$ . The island width,  $W_i$ , will be kept constant. That means that  $t$  must be shorter than the typical island growth<sup>46</sup>  $\tau_i = (\partial \ln W_i / \partial t)^{-1} \approx W_i \Delta' \tau_\eta$ , where  $\tau_\eta$  is the global resistive time scale.<sup>47</sup> Table 1 shows that this last requirement is consistent with previous time orderings. Width changes may then be treated adiabatically, i.e., the steady state Eq. (4) can be taken to be satisfied at all times as  $W_i$  is changed artificially.

The boundary condition on temperature encodes the influence of the island on the remaining of the plasma (and vice versa). To specify it, a simplified treatment of the energy dynamics of the rest of the tokamak is performed, using a steady state diffusion model like Eq. (1). It is convenient to apply Gauss' theorem to magnetic flux surfaces so that  $\int_{\psi} P dV = -\partial_{\psi} T \int_{\partial\psi} \kappa_i \hat{n} \cdot \nabla \psi dS$ , where  $\psi$  is the magnetic flux coordinate. This shows that the slope of the temperature profile at a particular flux surface is determined by the power deposited inside it. For simplicity, let us associate a spatial 1D coordinate  $R$ , in the absence of islands monotonic with  $\psi$ , and take the heat conductivity,  $\kappa_e$ , to be constant; then, the slope of temperature at some  $R_0$  is determined by the power deposited at  $R < R_0$ . With this in mind, let there be some heating in the tokamak center:  $P_c$  (fusion power, Ohmic heating, etc.) and  $P_{RF}$  (RF heating). The temperature profile is then determined by the heat flux and the fixed plasma edge temperature [see Fig. 1(a)].

Now, let there be an island of size  $W_i$  at a distance  $R_i$  from the core over which the temperature profile is flat [see Fig. 1(b)]. Because heat sources have not changed, the temperature slope remains unchanged elsewhere. Let then  $P_{RF}$  be redirected to the island (i.e., the

case of interest). For those magnetic flux surfaces at  $R > R_i + W_i/2$ , the enclosed total power does not change, and thus, the slope of  $T$  should neither [see Fig. 1(c)]. Given that the tokamak plasma edge temperature is fixed, the temperature at the edge of the island,  $T_0$ , remains unchanged. The boundary condition for our island temperature may then be taken to be  $\tilde{T}(x = \pm W_i/2) = 0$ .

It is now the turn of specifying  $P$  in Eq. (4) to represent the energy deposition from RF waves. Adopting a geometrical optics (GO) description of the wave envelope,<sup>48</sup> the evolution of the energy of the wave may be written as

$$d_t \bar{V} = \left[ -(\nabla \cdot v_g) + \frac{\omega_t}{\omega} + 2\gamma \right] \bar{V} \approx 2\gamma \bar{V}, \quad (5)$$

where  $\bar{V}$  represents the wave energy density,  $v_g$  is the group velocity of the wave,  $\omega_t$  represents the time derivative of frequency due to a time dependent medium,  $d_t$  represents the total time derivative following a wave along a ray, and  $\gamma$  represents the collisionless damping rate. Assuming the medium to be stationary in the wave damping time scale ( $\omega/\omega \ll \gamma$ ) and the spatial inhomogeneity to be much smaller than the variation resulting from the damping ( $\nabla \cdot v_g \ll \gamma$ ), the last approximated equality follows. This condition is not difficult to satisfy, considering only small variations are created within the island.

Expressing Eq. (5) in terms of  $x$ , the distance along the ray  $d_{tx} = v_g$ ,

$$d_x \bar{V} = 2 \frac{\gamma}{v_g} \bar{V}, \quad (6)$$

which has the form of damped propagation. The factor  $\gamma$  may be obtained under the assumption of a Maxwellian magnetized background;<sup>38,49</sup> one may show that for EC and LH,  $\gamma \propto \exp(-\chi^2)$ , where  $\chi = (\omega - n\Omega_e)/k v_{Te} = v_{\parallel}/v_{Te}$ , where  $v_{\parallel}$  is the phase velocity of the wave,  $v_{Te}$  is the electron thermal speed,  $\Omega_e$  is the electron cyclotron frequency, and  $n=0$  corresponds to LH waves and  $n=-1$  to EC waves. The power deposition for both electron cyclotron and lower hybrid waves occurs on the tail of the Maxwellian velocity distribution, with damping exponentially small in the lowest resonant velocity.

It is this exponential factor which makes deposition highly sensitive to variations in temperature. Indeed, considering the phase velocity of the wave to remain constant over the extent of the island,

$$\gamma \propto e^{-(v_{\parallel}/v_{Te,0})^2} \exp\left(\frac{v_{\parallel}^2 \tilde{T}}{v_{Te,0}^2 T_0}\right) \rightarrow \frac{2\gamma}{v_g} = -\alpha e^u.$$

It is convenient here to define the dimensionless variable  $u \equiv v_{\parallel}^2 \tilde{T} / v_{Te,0}^2 T_0 = w^2 \tilde{T} / T_0$ , where  $w = v_{\parallel} / v_{Te,0}$ . The location of the wave damping within the whole plasma is generally dependent on  $T$ ,  $B$ ,  $\omega$ , and  $k$ . This location can be determined using ray tracing.<sup>50,51</sup> Here, the picture is simplified by artificially restricting the damping to a particular defined region within the island, while keeping  $v_{\parallel}$  constant, and that way allowing for the  $\tilde{T}$  expansion. A fully self-consistent, full GO analysis is left for future work.

Let us express Eq. (6) as

$$d_x \bar{V} = -\alpha(x) e^u \bar{V}, \quad (7)$$

where the damping strength  $\alpha(x) \equiv 2\alpha_0 f(x)/W_i$ . The factor  $\alpha_0$  represents the strength of the damping, but it is also defined in a

dimensionless way to include the island width  $W_i$ . For example, for EC waves,<sup>38</sup>  $\alpha_0 \approx W_i \sqrt{\pi} \omega_{pe}^2 \exp(-w^2)/2ckv_{Te}$ . It is helpful to introduce a more physically motivated interpretation of  $\alpha_0$ . If a linear limit is taken of Eq. (7), the power deposition profile takes the form  $|V'| \propto \exp(-2\alpha_0 x/W_i)$ , i.e.,  $\alpha_0$  is the ratio of the island half-width to the characteristic deposition width. Note that the deposition has an exponential shape and not its usual Gaussian form generally considered for electron-cyclotron waves;<sup>50</sup> however, both schemes are peaked and of finite width and ultimately quite similar.

Now, going back to the original question: how is  $P$  related to this wave energy  $\bar{V}$ ? From the damping of the wave along a ray, it is easily seen that the volumetric power deposition at a given point is given by  $P = -d_t \bar{V} \approx -v_g d_x \bar{V} \equiv -v_g \bar{V}'(x)$ . However, because in this particular geometry the points  $\pm x$  are linked together (recall this is true due to them belonging to the same flux surface), these points share the total deposition at  $x$  and  $-x$ . All things considered

$$-\kappa_{\perp} \partial_x^2 \bar{T}(x) = -v_g \frac{\bar{V}'(x) + \bar{V}'(-x)}{2}, \quad (8a)$$

$$\bar{V}'(x) = -\alpha(x) e^u \bar{V}(x). \quad (8b)$$

These equations may be nondimensionalized, reducing them to

$$V'(\tilde{x}) = -f(\tilde{x}) e^u V(\tilde{x}), \quad (9a)$$

$$u'' = \frac{V'(\tilde{x}) + V'(-\tilde{x})}{2}, \quad (9b)$$

where the new  $V(\tilde{x}) = \bar{V}(x) W_i v_g v_p^2 / 2\alpha_0 \kappa_{\perp} T_0 v_T^2 = \bar{V}(x) W_i \Upsilon^2 / \alpha_0$  and  $\tilde{x} = 2\alpha_0 x / W_i$ . Note that the edges are now at  $x = \pm \alpha_0$ .

In order to complete the setting of the problem, an initial value must be taken for Eq. (9a). Let  $V_X \equiv V(-\alpha_0) \equiv V_0 / \alpha_0$ , where  $V_0$  is a constant representing some wave energy density input. For interpreting solutions, it is important to bear in mind that  $V_X$  is independent of the island width but will, however, scale as  $1/\alpha_0$  with the deposition strength.

For clarity in the following Secs. III and IV, one may refer to Appendix B as a quick reference for the variables employed.

### III. HYSTERESIS PHENOMENA

To investigate the effect of the nonlinear wave deposition, consider the tractable basic problem of wave damping occurring everywhere within the island. This case, represented by  $f(\tilde{x}) = 1$ , allows for an analytical solution of Eqs. (9a) and (9b) (see Appendix A for a detailed derivation). Implementing the appropriate boundary and initial conditions,

$$u(\tilde{x}) = 2 \log \gamma - \log \left[ \sqrt{(\lambda + 1)^2 - \gamma^2 \cosh \gamma \tilde{x}} + (\lambda + 1) \right], \quad (10)$$

where the parameters  $\lambda$  and  $\gamma$  are determined by

$$[\gamma^2 - (1 + \lambda)]^2 = \cosh^2(\alpha_0 \gamma) [(\lambda + 1)^2 - \gamma^2], \quad (11a)$$

$$\gamma^2 = (2\lambda + 1) + (V_X - \lambda)^2. \quad (11b)$$

The integration constant is  $\lambda = (V_X + V_f)/2$ , where  $V_f$  is the energy density when exiting the island. Equations (11a) and (11b) solve  $\lambda$  implicitly, which ultimately determines the temperature of the island as a function of  $\alpha_0$  and  $V_X$  from Eq. (10).

The dependence of perturbed central island temperature on these two parameters will be represented as contour curves (see, for example, Fig. 2). Two main representations are of particular physical interest. First, contours of constant  $\alpha_0$  (i.e., fixed deposition strength and island width) in the  $u(0) - V_0$  plane. These contours show the effects of the wave power on temperature [see Fig. 2(a)]. The second interesting picture is related to how the heating of the island evolves as its width or the wave profile width changes. This is captured by curves of constant  $V_X$  or  $V_0$  at fixed deposition strength in the  $u(0) - \alpha_0$  plane [see Fig. 2(b) for example].

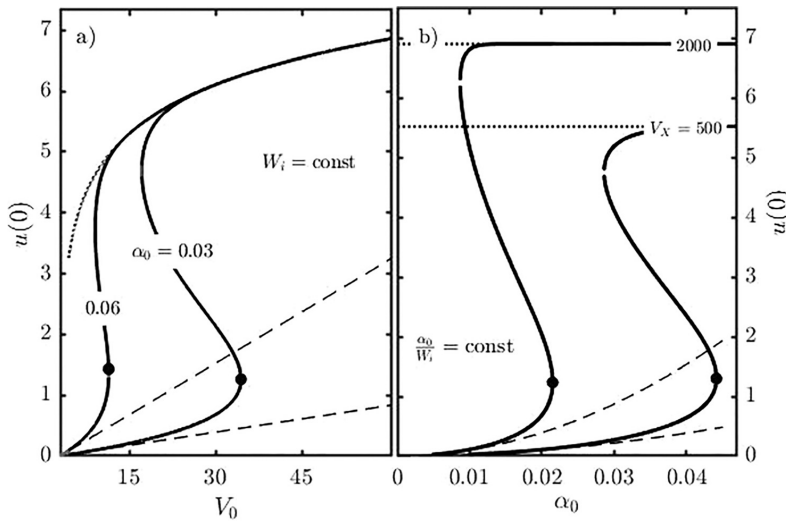


FIG. 2. (a) Island temperature at fixed deposition strength for different island widths, as a function of absorbed RF power, showing the appearance of the bifurcation point (shown bigger points). Dashed lines correspond to the linear limit of the solution; the dotted line corresponds to the asymptotic form of the solution for almost complete power deposition. (b) Central island temperature with varying island widths for constant incident wave energy densities  $V_X$ . The broken lines represent the solution to the linear problem while the dotted ones the asymptotic limit solution for complete energy deposition.

There are a number of general features in the solutions to Eqs. (10)–(11b) worth highlighting. The first of those is the existence of bifurcation points. As previously observed,<sup>41</sup> for sufficiently broad depositions (small  $\alpha_0$ ), saddle-node bifurcations appear, at which the two lower temperature solutions disappear. Such points are marked in Fig. 2(a). The appearance of these points may be linked to the action of a self-focusing mechanism affecting RF waves. Schematically, below the bifurcation, significant energy leakage takes place. As the bifurcation is approached, island temperature perturbations become larger, while the power deposited by the wave increases accordingly. This positive feedback eventually extracts all RF energy effectively, reaching a higher temperature steady state and thus jumping into an upper branch of the solution.

This hot stable solution may be seen in Fig. 2, along with the asymptotic form of the solution as  $V_f \rightarrow 0$  (dotted line). The proximity of the two solutions demonstrates that the upper branch indeed corresponds to nearly complete deposition of the wave energy in the island. Such a solution branch is also, immediately after the bifurcation point, significantly larger than the linear prediction (see broken lines).

A consequence of the solution structure obtained is the hysteresis behavior of island heating. To illustrate such a process, take as a starting point the system to be in equilibrium at the lower temperature branch in Fig. 2(a) and increase the absorbed energy of the incoming wave ( $V_0$ ) gradually. As a result, the temperature of the island will grow until the bifurcation point is reached. Once at this point, and driven by the self-focusing feedback, the temperature of the island will rapidly increase toward the upper branch, which is the only stable solution at high absorbed power.

The hot island exhibits, at this point, a large temperature difference between its center and the separatrix. *A priori*, this would help RF power to be absorbed closer to the O-point and thus also drive current,  $j$ , more centrally.<sup>44</sup> For this work, we take the driven current distribution to be proportional to the power deposition profile, thus assuming that, to leading order, the current drive efficiency is constant throughout the island. In the present work, we ignore currents associated with the DC electric field, which could arise due to changes in Spitzer conductivity or the hot electron conductivity.<sup>52,53</sup> These currents are less important than the directly driven RF current.<sup>41</sup>

With such presumed centered current drive, the island would tend to shrink and stabilize, as described by the 0D Rutherford equation.<sup>47</sup> This size reduction corresponds to a leftward displacement toward smaller values of  $\alpha_0$  in Fig. 2(b). In such a case, and if the energy available to the island is maintained, the reduction does not imply a return back to the original low temperature but instead remains in the more effective current driving upper branch for some time. Similarly, once in the upper branch, driving power requirements are relaxed, and lower  $V_0$  would still keep the plasma hot. This constitutes the hysteresis effect. A more careful discussion on the usefulness, accessibility, and consistency of this sketched simplified picture for particular deposition schemes is the concern of Sec. IV.

#### IV. EFFECTS OF NONLINEAR FEEDBACK

##### A. Typical parameters

Before proceeding further, a brief estimate and collection of typical values for both  $V_0$  and  $\alpha_0$  are presented. We emphasize that our slab model provides a physical qualitatively correct picture of the problem, but only a rough guide into the quantitative behavior of the

more realistic geometry, as previous calculations suggest.<sup>41</sup> Other simplified features, such as the exponential form of the linear deposition profile, are also different when compared to actual experiments<sup>50</sup> but do, however, share the fundamental characteristics. Thus, the linear case will be taken as a reference in guiding conclusions, as well as an orientative comparison standard to existing experimental parameters.

Focus first on the values for the parameter  $\alpha_0$ . Two different routes are taken at this point. One possible method uses, given the definition of  $\alpha_0$  as the size of the linear power deposition width, typical deposition widths in tokamak experiments which could be used to obtain  $\alpha_0 \sim 0.5$ – $3$ .<sup>42</sup> It has been recently reported that current drive profiles are in experiment subject to broadening<sup>54</sup> by factors of 2–3 due to effects unaccounted for in ray tracing routines, such as edge density fluctuations. This effective broadening could make typical  $\alpha_0$  values even lower, down to  $\sim 0.2$ .

Alternatively, one could use the form for  $\alpha_0$  given before and obtained in the context of GO. In the case of ECCD, for instance, using typical approximated hydrogen tokamak values (see the caption of Table I), with  $w^2 \sim 10$ ,<sup>38</sup> wavenumber<sup>55</sup>  $k \sim 2\pi/(5 \text{ mm})$ , density  $n \sim 10^{20} \text{ m}^{-3}$ , and  $W_i \sim 10 \text{ cm}$ ;  $\alpha_0 \approx W_i \sqrt{\pi} \omega_{pe}^2 \exp(-w^2) / 2ckv_{Te} \sim 10^{-1}$ .

Now, consider the wave power density  $V_0$ . First, we note that numerical calculations of island temperature variations reported in the literature<sup>42</sup> are already, for certain cases, on the order of 25% for powers on the order of 20 MW. This corresponds to  $V_0 \sim 5$  in the linear low-power limit of our model. Alternatively, we could arrive at typical  $V_0$  values by relating the analytical expression for the heat diffusion to the power deposition. This gives  $V_0 \approx PW_i w^2 / 2A \chi_{\perp} n k_B T_0 \sim 10^1$ , where we took RF power to be on the order of  $P \sim 10 \text{ MW}$ , with a beam of cross section  $A \sim 1 \text{ m}^2$ , with  $\chi_{\perp} \sim 1 \text{ m}^2/\text{s}$ , temperature  $T_0 \sim 10 \text{ keV}$ , density  $n \sim 10^{20} \text{ m}^{-3}$ , and  $w^2 \sim 10$ .

Summarizing,

$$\alpha_0 \sim 0.1 - 3 \quad V_0 \sim 10^1. \quad (12)$$

##### B. Central deposition

The spatial distribution of the RF deposition strongly affects the final temperature of the island, as well as the island mitigation efficiency. In this section, the best case scenario is first analyzed, i.e., deposition starting from the island center. To formally emulate this ideal case,  $f(\vec{x}) = H(\vec{x})$ , where  $H$  is the Heaviside step function. Given this newly introduced asymmetry, well defined parity is lost from the equations and the solution to the equation is only found numerically.

Consider first the occurrence of bifurcation points and, in particular, how they depend on  $\alpha_0$ . To illustrate these points, Figs. 3 and 4 are presented.

In the broad linear deposition limit, with  $3\alpha_0 \ll 1$ , there always exists a bifurcation point (see Fig. 3). The turning point, however, occurs at increasingly larger wave energy densities  $V_0$ . One may understand this result by referring to the analytical asymptotic form of the solution at low  $V_0$ . In that limit, the system takes the form of the linear problem, for which  $u(0) \sim V_0(\alpha_0 - 1 + e^{-\alpha_0})/2\alpha_0$ . This shows that the temperature of the island becomes decreasingly responsive as  $\alpha_0 \rightarrow 0$  (see the decreasing initial slopes of curves in the inset of Fig. 3), which is ultimately related to there being a significant wave energy leakage ( $V_f = V_{\chi} e^{-\alpha_0}$ ).

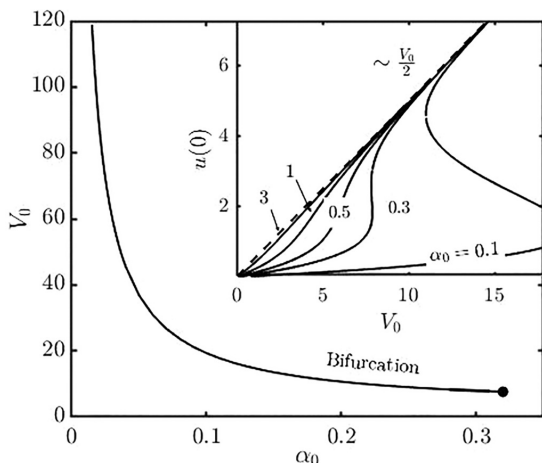


**FIG. 3.** Wave power density value for the bifurcation at a given deposition strength  $\alpha_0$ , for deposition starting at the island center. The larger scatter point represents the limiting value of  $\alpha_0$  over which no bifurcation exists. The inset shows curves of constant deposition strength in the  $u(0) - V_0$  plane. The broken line represents the asymptotic form of the nonlinear solution.

Only for those cases for which the initial energy leakage  $V_f$  is significant will a bifurcation occur. The bifurcation is a result of the system being able to access all that previously lost energy when the damping  $e^u$  factor becomes significant. This jump will be associated

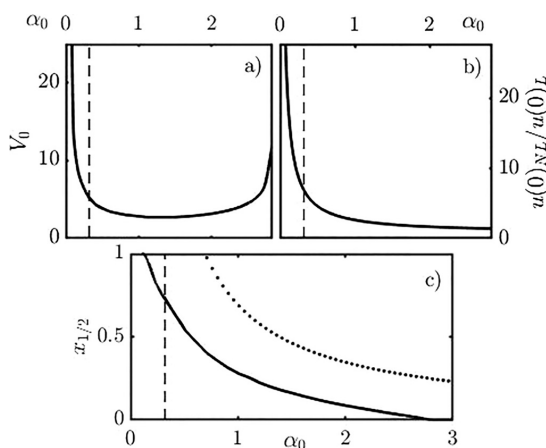


**FIG. 4.** (a) Wave power density value for 50% difference between the linear and nonlinear solutions for centered wave energy deposition. (b) Upper bound to ratio of nonlinear to linear island temperature. (c) Power deposition half-peak width  $x_{1/2}$  for the points in the curve in (a) (continuous line) and for the linear equivalent problem (dotted line) for  $\alpha_0 > 0.1$ . Solutions for the region  $\alpha_0$  to the left of the broken line represent solutions with existing bifurcation points. For  $\alpha_0 \approx 2.8$ , the nonlinear deposition profile becomes similar to that of a delta function (within discretization) as  $V_0 \rightarrow \infty$ .

with a narrowing of the deposition and a current that is more efficiently utilized in stabilization.

As the initial deposition is reduced by increasing  $\alpha_0$ ,  $V_f$  in the lower branch decreases, and it eventually becomes too small to sustain a bifurcation. Figure 3 shows the boundary value  $\alpha_0 = 0.32$  beyond which no bifurcation occurs.

Where no bifurcation occurs, the temperature of the island only undergoes a smooth transition in temperature between the linear solution and the high temperature asymptote (see Fig. 3). That limiting form of the nonlinear solution as  $V_f \rightarrow 0$  is  $u(0) \sim V_0/2$  (see the dashed line in the inset of Fig. 3 and Appendix C), which is also the limit as  $\alpha_0 \rightarrow \infty$  of the linear deposition. That is, the nonlinear response serves as a short cut via self-focusing to the linear ideal infinitely narrow deposition. Thus, for the case of centralized deposition, the nonlinear mechanism always leads to an enhanced temperature increase.

However, the wave power required to obtain a substantial improvement exhibits a strong dependence on  $\alpha_0$  as shown in Fig. 4(a). The large energy leakage and the small difference between linear and nonlinear solutions at low and high  $\alpha_0$ , respectively, leave a most easily accessible (lower  $V_0$ ) central region at values  $\alpha_0 \sim 1-1.5$ . To emphasize the second of these limitations, Fig. 4(b) shows the ratio of the analytical asymptotic forms of the nonlinear and linear solutions. Evidently, the differences become marginal (i.e., the ratio tends to one) for stronger depositions, which explains why Fig. 4(a) diverges at  $\alpha_0 \sim 2.8$ .

Finally, we examine the extent to which the self-focusing mechanism narrows RF deposition. Figure 4(c) serves as an example of the clear narrowing of the deposition, which undoubtedly improves stabilization as current drive is brought closer to the O point. More generally, one may estimate the deposition width assuming that the island temperature takes its asymptotic form at large powers. In that case, using the form for  $|V'| = V_0 e^u \exp(-\int e^u dx)$  and assuming that the deposition width,  $\Delta x$ , is narrow compared to the island width,  $|V'| \sim V_0 e^{u(0)} \exp(-e^{u(0)} \Delta x)$ , then the deposition width normalized to the linear deposition is  $\Delta x \sim \exp(-V_0/2)$ . This shows the exponential narrowing of the deposition profile (and hence the current drive) resulting from the temperature perturbations, which will tend to concentrate as one increases the input power or the island width  $W_i$  (as  $V_0 \propto W_i$ ).

This analysis suggests that the region of interest and current experimental relevance may in some subset of cases (for the broadest depositions) show some hysteresis behavior, but most will just show a significantly modified temperature and deposition distribution. In addition, as a result of the strong narrowing due to temperature, islands could be stabilized when traditionally predicted not to. This opens the door to experimental verification of the nonlinear effect, as well as extension of island stabilization schemes.

### C. Edge deposition

The scenario adopted for analysis before was that of central deposition. This is the ideal case, and so it presumes that one is experimentally capable of aiming perfectly at the center of the island without depositing any energy before that. However, what would happen if the deposition departs from this idealized case? The worst case scenario is now presented. To that end, we recover the analytical solution from Eqs. (10)–(11b), which represents wave deposition from the very edge of the magnetic island.

With this analytical result at hand, let us explore first the limit of complete wave deposition:  $u(0) \sim \log(V_0/2\alpha_0 + 1)$ . The linear solution gives  $u(0) = V_0 e^{-2\alpha_0} (\cosh \alpha_0 - 1) / \alpha_0$ . It is remarkable that the nonlinear model gives a logarithmic growth of the island temperature as the power input is increased, while the linear case grows linearly. It necessarily follows that some nonlinear inhibition mechanism must be present. Indeed, one may relate this to the deposition profile becoming localized ever closer to the edge of the island.

It is the same self-focusing that narrowed the deposition closer to the center when central deposition was considered, which displaces deposition toward the island edge (see Fig. 6). Physically, the RF wave becomes so strongly damped that it runs out of energy very close to the edge before penetrating. There, the temperature slope is large, and thus, heat gets quickly lost across the edges,  $u(0)$  becoming limited.

As a result of this detrimental displacement, only over a limited regime will the nonlinear solution be hotter than the linear one. As shown in Fig. 5, this interval is larger for the broader depositions but tends to disappear as  $\alpha_0 \rightarrow \infty$ . This is a result of the nonlinear focusing being able to increase the amount of deposited power significantly, thus allowing for the focusing benefits to outweigh the inhibition for a wider range of powers.

In addition to temperature, this deposition shift will also bring the driven current closer to the X-point. This displacement can be catastrophic when trying to suppress the growth of magnetic islands as described by the 0D Rutherford equation. The proximity of the deposition to the edge may be seen in Fig. 6. For typical values  $\alpha_0 \sim 1$  and  $V_0 \sim 5-10$ , the peak of deposition  $x_{\text{peak}} \sim -0.7$ , i.e., power is deposited somewhere between the X- and O-points. The plot shows that in general, there are two stages to the deposition peak location dynamics: one at large  $V_0$  values, for which the nonlinear self-focusing brings the deposition ever

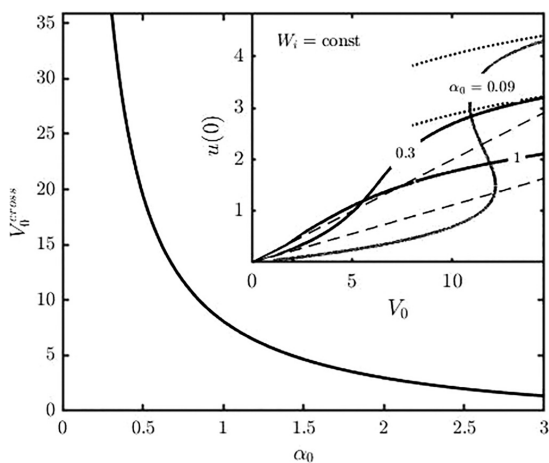


FIG. 5. Power at which the nonlinear and linear solutions give the same central temperature with deposition starting from the edge, as a function of the deposition strength. The region to the left of the curve represents the case for larger nonlinear solution. The inset shows examples of constant deposition curves as a function of power. The broken lines represent the linear solution, while the dotted curves show the logarithmic asymptotic behavior of the nonlinear one.

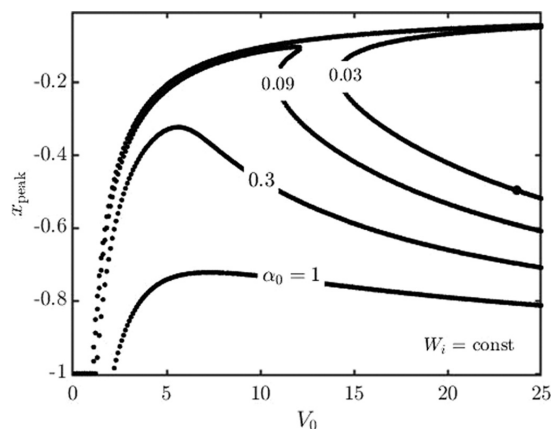


FIG. 6. Location of the power deposition peak as a function of power for various deposition strengths (complementary to Fig. 5). A value of  $x_{\text{peak}} = 0$  corresponds to a centered deposition, while a value of  $-1$  represents the edge.

closer to the edge. This is the result of the large damping  $e^{u'}$  draining the incoming wave faster than  $V_0$  increases. The other stage corresponds to a lower  $V_0$  region in which the focusing is starting to affect the system, drawing the power toward the center, and minimizing leakage.

To further explore the sensitivity of stability on  $x_{\text{peak}}$ , the procedure in Ref. 15 is followed. The relative Fourier weighting to  $\Delta'$  in the 0D Rutherford equation due to driving current at a particular flux coordinate,  $\psi$  ( $\Omega$  in the reference), may be estimated taking the 1D spatial variable  $x$  in our model to match the spatial  $x$  in Ref. 15, looking at  $\xi = 0$  (see Fig. 7). The calculation shows that within approximately 90% of the island, the drive is stabilizing. Therefore, looking back at Fig. 6, the current drive will still be central enough to be stabilizing for

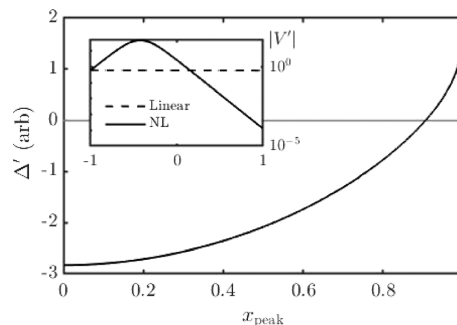


FIG. 7. Scaled contribution to  $\Delta'$  in the Rutherford equation due to current drive at different positions within the island. Current drive is stabilizing for  $\Delta' < 0$ , i.e., when driving is roughly within 90% of the island extent. The inset shows the deposition profiles for the linear and nonlinear solutions corresponding to the point shown in Fig. 6, represented on a log scale (the linear deposition is almost uniform but the largest at the X point).

a significant fraction of the cases, even when the nonlinear solution is colder than the linear one. No definitive conclusion may, however, be drawn on the precise fraction of the island that is truly stabilizing, as the treatment of the island geometry in Ref. 15 is different from that of our model. A fully consistent treatment is left for future work.

We have shown that an initially broad RF profile may then be used to stabilize islands, so long as the input power remains below some upper bound thanks to the self-focusing of the RF. This result is promising and an idea to further explore.

More generally, if deposition was to start midway between the X- and O-points, then deposition would be driven and narrowed toward that location instead. The trends will then fit between the extreme center and edge cases shown explicitly, with less constraining requirements as the center is reached. In this context, RF overshooting scenarios will never suffer from the inhibition that takes place when undershooting with increasing  $V_0$ .

Yet another possibility to circumvent inhibition might be to look for means to amplify the wave power within the island, such as through an  $\alpha$ -channeling effect.<sup>56</sup> This could give a power not peaked at the island periphery. Unfortunately, this volumetric amplification does not occur for electron cyclotron waves but might be exploited when using lower hybrid waves.<sup>57</sup> Despite lacking this possible enhancement, EC waves do, however, have the benefit of having a  $B$ -dependent resonance that allows for deposition starting at a particular point in space.

### V. DISCUSSION AND CONCLUSIONS

The possibility of hysteresis involving the heating of magnetic islands with RF waves is shown for a symmetrized, 1D slab model. Our slab model gives a rough guide to the quantitative behavior of the more realistic full-geometry model. Accordingly, the wave power deposition self focuses mediated by island temperature, leading to higher temperatures. Past a bifurcation point, the island may remain in this high temperature solution even as it shrinks or power is reduced. Exploiting the hysteresis effect could thus provide an easier and improved way to eliminate magnetic islands.

It predicts that, in typical parameter regimes of current experiments, a bifurcation is likely to occur for the broadest electron cyclotron profiles. It should be noted that lower hybrid profiles are typically broader than EC profiles. Even in the absence of such bifurcations, centered deposition scenarios show that important temperature increments (on the order of  $\sim 50\%$ ) occur. These differences are, again, most significant in broader deposition schemes, where the self-focusing mechanism of the nonlinear model is most different from the linear model.

Considering the effects of temperature on the deposition, and hence also the RF current drive, profiles are shown to be significantly narrowed, a reduction that scales exponentially with power and island width. This will improve its utility for purposes of stabilization. Though not shown here, temperature perturbations could in addition lead to enhanced stabilization through a modified peaked conductivity.<sup>41</sup>

For broad deposition schemes that deviate from the center, not dissimilar self-narrowing and stabilization effects take place under certain circumstances. These circumstances involve the form of EC power density profiles and must be considered in designing deposition scenarios. In particular, for deposition profiles that peak before the O-point, there is a threshold power density above which a self-inhibition mechanism is encountered; beyond the O-point, this threshold does not exist. This suggests that it will be important to take

into account nonlinear effects in determining the optimal aiming of trajectories. It also opens the door to exploring previously disregarded broad RF deposition stabilization schemes.

The hysteresis effect explored here requires only that there is a nonlinear current condensation effect limited by some constraint that halts condensation. The limiting effect explored here was the availability of RF power, which is a natural physical limitation to include. There could, in principle, be other phenomena that arise more importantly or possibly in addition to the power availability, such as radiation from impurities, nonlinear temperature effects on the transport, or nonlinear temperature effects that cause deflection of the RF waves. Although these effects would change the details of the hysteresis effect, the effect itself should still persist. Similarly, a more detailed and self-consistent calculation of the ray trajectories would tend to modify, but not change in character, the hysteresis phenomena observed here.

Another caveat is that the model employed here is a 1D slab model; more quantitative calculations would consider the 2D or 3D effects that attend toroidal and specific magnetic island geometry. Also, considerations of more general island growth behavior,<sup>22</sup> beyond what is captured in the 0D Rutherford model employed here, could affect the findings here as well.

### ACKNOWLEDGMENTS

The authors thank Suying Jin and Daniel Korsun for fruitful discussions and help.

This work was supported by Nos. U.S. DOE DE-AC02-09CH11466 and DE-SC0016072.

### APPENDIX A: ANALYTICAL SOLUTION TO CONSTANT $\alpha$

Consider the coupled set of equations,

$$V'(\tilde{x}) = -e^u V(\tilde{x}), \tag{A1a}$$

$$u'' = \frac{V'(\tilde{x}) + V'(-\tilde{x})}{2}, \tag{A1b}$$

subject to the conditions shown in Table II. Define the following symmetric and antisymmetric parts of the wave energy density,

$$S = \frac{V(\tilde{x}) + V(-\tilde{x})}{2}, \tag{A2}$$

$$A = \frac{V(\tilde{x}) - V(-\tilde{x})}{2}. \tag{A3}$$

Given these, Eq. (A1b) may be cast in the form,

TABLE II. Initial conditions that specify the problem that is to be solved.

Var	$\tilde{x}$ limit	Var limit
$u$	$-\alpha_0$	0
$u'$	0	0
$V$	$-\alpha_0$	$V_X$
$V'$	$-\alpha_0$	$-V_X$

$$u'' = \left[ \frac{V(\bar{x}) - V(-\bar{x})}{2} \right]' = A'. \quad (\text{A4})$$

Substituting definitions (A2) and (A3) into Eq. (A1a),

$$(A + S)' = -e^u(A + S),$$

and realizing that the spatial derivative  $\frac{d}{d\bar{x}}$  is an odd operator while  $u$  is an even function, the equation may be separated into its symmetric and asymmetric parts,

$$S' = -e^u A, \quad (\text{A5})$$

$$A' = -e^u S, \quad (\text{A6})$$

which with Eq. (A4) form a set of three coupled nonlinear differential equations. The set avoids the explicit appearance of  $-x$  on the expense of an additional equation.

Because of even parity,  $u'(\bar{x} = 0) = 0$ , and so Eq. (A4) may be integrated as

$$u' = A. \quad (\text{A7})$$

Substituting (A7) and (A4) into Eqs. (A5) and (A6), putting together, and integrating once,

$$u'' = e^u [e^u - (1 + \lambda)], \quad (\text{A8})$$

where  $\lambda$  is an integration constant that must satisfy the initial conditions specified. From Eq. (A4), it follows that  $\lambda = (V_X + V_f)/2$ , which limits  $V_X/2 < \lambda < V_X$ .

To solve Eq. (A8), multiply both sides of the equation by  $u'$  and integrate with respect to  $\bar{x}$ . Thus,

$$u'^2 = e^u [e^u - 2(\lambda + 1)] + C, \quad (\text{A9})$$

where  $C$  is another integration constant to be determined later on.

Let the substitution  $u \equiv -\log z$  be implemented in Eq. (A9),

$$z'^2 = 1 - 2(\lambda + 1)z + Cz^2. \quad (\text{A10})$$

At his point, one may try a symmetric solution of the form  $z = A(e^{\gamma\bar{x}} + e^{-\gamma\bar{x}}) + B$ , where  $A$ ,  $B$ , and  $\gamma$  are to be reduced to a single integration constant. If this is possible, uniqueness guarantees this to be the general solution. After some manipulation,

$$C = \gamma^2, \quad B = \frac{\lambda + 1}{\gamma^2}, \quad A^2 = \frac{(\lambda + 1)^2 - \gamma^2}{4\gamma^4}, \quad (\text{A11})$$

which indeed leaves a single degree of freedom,  $\gamma$ , as expected for a first order ODE. It is then time to implement boundary conditions to determine  $\lambda$  and  $\gamma$ . From  $u = 0$  at  $\bar{x} = -\alpha_0$ ,  $z(\bar{x} = -\alpha_0) = 1$  is evaluated, and eliminating  $A$ ,

$$[\gamma^2 - (1 + \lambda)]^2 = \cosh^2 \alpha_0 \gamma [(\lambda + 1)^2 - \gamma^2]. \quad (\text{A12})$$

Having eliminated  $A$ , the solution for  $u$  is as follows:

$$u(\bar{x}) = 2 \log \gamma - \log \left[ \sqrt{(\lambda + 1)^2 - \gamma^2} \cosh \gamma \bar{x} + (\lambda + 1) \right]. \quad (\text{A13})$$

The additional boundary or initial condition may be imposed requiring  $u'(-\alpha_0) = A(-\alpha_0) = (V_X - V_f)/2 = V_X - \lambda$  from Eq. (A8), which will introduce explicitly the physically relevant parameter  $V_X$ . Then,

$$\gamma^2 = (2\lambda + 1) + (V_X - \lambda)^2, \quad (\text{A14})$$

where  $\gamma^2 > 1 + 2\lambda$ .

TABLE III. Reference description of variables in Secs. III and IV.

$\bar{x}$	Dimensionless position
$u$	Dimensionless temperature variations
$T_0$	Background temperature
$u(0)$	$u$ at the island center
$V$	Dimensionless wave energy density
$V_X$	$V$ at the left X-point
$V_0$	Scaled $V_X$ : $V_0 = \alpha_0 V_X$
$V_f$	$V$ leaving island
$\alpha_0$	Half island to deposition width (also island edges)
$\alpha_0/W_i$	Deposition strength
$W_i$	Island width
$x_{\text{cent}}$	Deposition midpoint location
$w$	Ratio phase to thermal speeds
$\omega$	RF frequency

## APPENDIX B: SUMMARY OF VARIABLES AND ABBREVIATIONS

A collection of the variables used in Secs. III and IV is presented as a reference in Table III. A brief description is also provided where relevant.

## APPENDIX C: ASYMPTOTIC LIMIT NONLINEAR CENTRAL DEPOSITION

Let us consider the limiting case for complete RF power deposition in island stabilization starting deposition from the center of the magnetic island.

Begin with

$$u'' = \frac{V'}{2} \rightarrow u' = \frac{V}{2} - \frac{V_X}{2}. \quad (\text{C1})$$

Now take the wave energy to be damped quickly so that  $V \approx 0$  for  $x > 0$ . In that case, and as the edge is located at  $x = \alpha_0$ ,

$$u(0) \sim \alpha_0 \frac{V_X}{2}. \quad (\text{C2})$$

## REFERENCES

- <sup>1</sup>Z. Chang, J. D. Callen, E. D. Fredrickson, R. V. Budny, C. C. Hegna, K. M. McGuire, and M. C. Zarnstorff, *Phys. Rev. Lett.* **74**, 4663 (1995).
- <sup>2</sup>R. J. LaHaye, L. L. Lao, E. J. Strait, and T. S. Taylor, *Nucl. Fusion* **37**, 397 (1997).
- <sup>3</sup>H. Zohm, D. A. Gates, H. R. Wilson, G. Gantenbein, O. Gruber, S. Gunter, M. Maraschek, A. W. Morris, M. Sokoll, D. Wagner, A. U. Team, and C.-D. Team, *Plasma Phys. Controlled Fusion* **39**, B237 (1997).
- <sup>4</sup>D. A. Gates, B. Lloyd, A. Morris, G. McArdle, M. O'Brien, M. Valovic, C. Warrick, H. Wilson, COMPASS D Team, and ECRH Team, *Nucl. Fusion* **37**, 1593 (1997).
- <sup>5</sup>R. J. Buttery, S. Günter, G. Giruzzi, T. C. Hender, D. Howell, G. Huysmans, R. J. L. Haye, M. Maraschek, H. Reimerdes, O. Sauter, C. D. Warrick, H. R. Wilson, and H. Zohm, *Plasma Phys. Controlled Fusion* **42**, B61 (2000).
- <sup>6</sup>P. C. de Vries, M. Johnson, B. Alper, P. Buratti, T. Hender, H. Koslowski, V. Riccardo, and J.-E. Contributors, *Nucl. Fusion* **51**, 053018 (2011).
- <sup>7</sup>P. C. de Vries, M. Baruzzo, G. M. D. Hogewej, S. Jachmich, E. Joffrin, P. J. Lomas, G. F. Matthews, A. Murari, I. Nunes, T. Pütterich, C. Reux, J. Vega, and J.-E. Contributors, *Phys. Plasmas* **21**, 056101 (2014).

- <sup>8</sup>A. H. Reiman, *Phys. Fluids* **26**, 1338 (1983).
- <sup>9</sup>Y. Yoshioka, S. Kinoshita, and T. Kobayashi, *Nucl. Fusion* **24**, 565 (1984).
- <sup>10</sup>O. Sauter, *Phys. Plasmas* **11**, 4808 (2004).
- <sup>11</sup>R. Kamendje, S. V. Kasilov, W. Kernbichler, I. Pavlenko, E. Poli, and M. F. Heyn, *Phys. Plasma* **12**, 012502 (2005).
- <sup>12</sup>R. J. La Haye, *Phys. Plasmas* **13**, 055501 (2006).
- <sup>13</sup>R. J. La Haye, J. R. Ferron, D. A. Humphreys, T. C. Luce, C. C. Petty, R. Prater, E. J. Strait, and A. S. Welander, *Nucl. Fusion* **48**, 054004 (2008).
- <sup>14</sup>M. A. Henderson, R. Heidinger, D. Strauss, R. Bertizzolo, A. Bruschi, R. Chavan, E. Ciattaglia, S. Cirant, A. Collazos, I. Danilov, F. Dolizy, J. Duron, D. Farina, U. Fischer, G. Gantenbein, G. Hailfinger, W. Kasperek, K. Kleefeldt, J. D. Landis, A. Meier, A. Moro, P. Platania, B. Plaum, E. Poli, G. Ramponi, G. Saibene, F. Sanchez, O. Sauter, A. Serikov, H. Shidara, C. Sozzi, P. Spaeh, V. S. Udintsev, H. Zohm, and C. Zucca, *Nucl. Fusion* **48**, 054013 (2008).
- <sup>15</sup>D. De Lazzari and E. Westerhof, *Nucl. Fusion* **49**, 075002 (2009).
- <sup>16</sup>F. A. G. Volpe, M. E. Austin, R. J. La Haye, J. Lohr, R. Prater, E. J. Strait, and A. S. Welander, *Phys. Plasma* **16**, 102502 (2009).
- <sup>17</sup>O. Sauter, M. A. Henderson, G. Ramponi, H. Zohm, and C. Zucca, *Plasma Phys. Controlled Fusion* **52**, 025002 (2010).
- <sup>18</sup>N. Bertelli, D. De Lazzari, and E. Westerhof, *Nucl. Fusion* **51**, 103007 (2011).
- <sup>19</sup>B. A. Hennen, E. Westerhof, P. W. J. M. Nuij, M. R. de Baar, and M. Steinbuch, *Nucl. Fusion* **52**, 074009 (2012).
- <sup>20</sup>A. I. Smolyakov, A. Poye, O. Agullo, S. Benkadda, and X. Garbet, *Phys. Plasmas* **20**, 062506 (2013).
- <sup>21</sup>B. Ayten, E. Westerhof, and ASDEX Upgrade Team, *Nucl. Fusion* **54**, 073001 (2014).
- <sup>22</sup>D. Borgogno, L. Comisso, D. Grasso, and E. Lazzaro, *Phys. Plasmas* **21**, 060704 (2014).
- <sup>23</sup>F. A. Volpe, A. Hyatt, R. J. La Haye, M. J. Lanctot, J. Lohr, R. Prater, E. J. Strait, and A. Welander, *Phys. Rev. Lett.* **115**, 175002 (2015).
- <sup>24</sup>O. Fevrier, P. Maget, H. Luetjens, J. F. Luciani, J. Decker, G. Giruzzi, M. Reich, P. Beyer, E. Lazzaro, S. Nowak, and A. U. Team, *Plasma Phys. Controlled Fusion* **58**, 045015 (2016).
- <sup>25</sup>S. Wang and Z. W. Ma, *Phys. Plasma* **22**, 122504 (2015).
- <sup>26</sup>J. C. Li, C. J. Xiao, Z. H. Lin, and K. J. Wang, *Phys. Plasmas* **24**, 082508 (2017).
- <sup>27</sup>D. Grasso, E. Lazzaro, D. Borgogno, and L. Comisso, *J. Plasma Phys.* **82**, 595820603 (2016).
- <sup>28</sup>D. Grasso, D. Borgogno, L. Comisso, and E. Lazzaro, *J. Plasma Phys.* **84**, 745840302 (2018).
- <sup>29</sup>E. Poli, C. Angioni, F. Casson, D. Farina, L. Figini, T. Goodman, O. Maj, O. Sauter, H. Weber, H. Zohm, G. Saibene, and M. Henderson, *Nucl. Fusion* **55**, 013023 (2015).
- <sup>30</sup>S. Bernabei, A. Cardinali, G. Giruzzi, and M. Zabiego, *Nucl. Fusion* **38**, 87 (1998).
- <sup>31</sup>C. D. Warrick, R. Buttery, G. Cunningham, S. Fielding, T. Hender, B. Lloyd, A. Morris, M. O'Brien, T. Pinfold, K. Stammers, M. Valovic, M. Walsh, H. Wilson, and C. D. R. Teams, *Phys. Rev. Lett.* **85**, 574 (2000).
- <sup>32</sup>G. Gantenbein, H. Zohm, G. Giruzzi, S. Gunter, F. Leuterer, M. Maraschek, J. Meskat, Q. Yu, ASDEX Upgrade Team, and ECRH-Group AUG, *Phys. Rev. Lett.* **85**, 1242 (2000).
- <sup>33</sup>H. Zohm, G. Gantenbein, A. Gude, S. Gunter, F. Leuterer, M. Maraschek, J. Meskat, W. Suttrop, Q. Yu, ASDEX Upgrade Team, and ECRH Group, *Nucl. Fusion* **41**, 197 (2001).
- <sup>34</sup>A. Isayama, Y. Kamada, S. Ide, K. Hamamatsu, T. Oikawa, T. Suzuki, Y. Neyatani, T. Ozeki, Y. Ikeda, K. Kajiwara, and J. Team, *Plasma Phys. Controlled Fusion* **42**, L37 (2000).
- <sup>35</sup>R. J. La Haye, S. Gunter, D. A. Humphreys, J. Lohr, T. C. Luce, M. E. Maraschek, C. C. Petty, R. Prater, J. T. Scoville, and E. J. Strait, *Phys. Plasmas* **9**, 2051 (2002).
- <sup>36</sup>C. C. Petty, R. J. La Haye, T. C. Luce, D. A. Humphreys, A. W. Hyatt, J. Lohr, R. Prater, E. J. Strait, and M. R. Wade, *Nucl. Fusion* **44**, 243 (2004).
- <sup>37</sup>N. J. Fisch and A. H. Boozer, *Phys. Rev. Lett.* **45**, 720 (1980).
- <sup>38</sup>C. F. F. Karney and N. J. Fisch, *Nucl. Fusion* **21**, 1549 (1981).
- <sup>39</sup>N. J. Fisch, *Phys. Rev. Lett.* **41**, 873 (1978).
- <sup>40</sup>C. F. F. Karney and N. J. Fisch, *Phys. Fluids* **22**, 1817 (1979).
- <sup>41</sup>A. H. Reiman and N. J. Fisch, *Phys. Rev. Lett.* **121**, 225001 (2018).
- <sup>42</sup>E. Westerhof, A. Lazaros, E. Farshi, M. de Baar, M. de Bock, I. Classen, R. Jaspers, G. Hogeweij, H. Koslowski, A. Krämer-Flecken, Y. Liang, N. L. Cardozo, and O. Zimmermann, *Nucl. Fusion* **47**, 85 (2007).
- <sup>43</sup>S. I. Braginskii, *Rev. Plasma Phys.* **1**, 205 (1965).
- <sup>44</sup>N. J. Fisch, *Rev. Mod. Phys.* **59**, 175 (1987).
- <sup>45</sup>L. Spitzer and R. Härm, *Phys. Rev.* **89**, 977 (1953).
- <sup>46</sup>J. Wesson and D. Campbell, *Tokamaks* (OUP, Oxford, 2004).
- <sup>47</sup>P. H. Rutherford, *Phys. Fluids* **16**, 1903 (1973).
- <sup>48</sup>E. R. Tracy, A. J. Brizard, A. S. Richardson, and A. N. Kaufman, *Ray Tracing and Beyond: Phase Space Methods in Plasma Wave Theory* (CUP, 2014).
- <sup>49</sup>T. H. Stix, *Waves in Plasmas* (AIP, 1992).
- <sup>50</sup>R. Prater, D. Farina, Y. Gribov, R. Harvey, A. Ram, Y.-R. Lin-Liu, E. Poli, A. Smirnov, F. Volpe, E. Westerhof, A. Zvonkov, and ITPA Steady State Operation Topical Group, *Nucl. Fusion* **48**, 035006 (2008).
- <sup>51</sup>P. T. Bonoli and R. C. Englade, *Phys. Fluids* **29**, 2937 (1986).
- <sup>52</sup>N. J. Fisch, *Phys. Fluids* **28**, 245 (1985).
- <sup>53</sup>C. F. F. Karney, F. C. Jobses, and N. J. Fisch, *Phys. Rev. A* **32**, 2554 (1985).
- <sup>54</sup>M. W. Brookman, M. E. Austin, K. W. Gentle, C. C. Petty, D. E. Ernst, Y. Peysson, J. Decker, and K. Barada, *EPJ Web Conf.* **147**, 03001 (2017).
- <sup>55</sup>R. Prater, *Phys. Plasmas* **11**, 2349 (2004).
- <sup>56</sup>N. J. Fisch and J.-M. Rax, *Phys. Rev. Lett.* **69**, 612 (1992).
- <sup>57</sup>I. E. Ochs, N. Bertelli, and N. J. Fisch, *Phys. Plasmas* **22**, 082119 (2015).